

Dynamic navigation-guided robotic placement of zygomatic implants

Mohammed Y. Al-Jarsha^{a,b}, Yufeng Diao^c, Guodong Zhao^{c,d}, Muhammad A. Imran^c,
Ashraf F. Ayoub^{a,*}, Douglas P. Robertson^e, Kurt B. Naudi^a

^a Department of Oral Surgery, School of Medicine, Dentistry and Nursing, College of Medical, Veterinary and Life Sciences, University of Glasgow, Glasgow, United Kingdom

^b Department of Oral and Maxillofacial Surgery, College of Dentistry, University of Baghdad, Baghdad, Iraq

^c James Watt School of Engineering, University of Glasgow, Glasgow, United Kingdom

^d University of Manchester, Manchester, United Kingdom

^e Department of Restorative Dentistry, School of Medicine, Dentistry and Nursing, College of Medical, Veterinary and Life Sciences, University of Glasgow, Glasgow, United Kingdom

ARTICLE INFO

Keywords:

Robotic surgical procedures
Zygoma
Feedback
Calibration
Feasibility studies

ABSTRACT

Objectives: To assess the feasibility and accuracy of a new prototype robotic implant system for the placement of zygomatic implants in edentulous maxillary models.

Methods: The study was carried out on eight plastic models. Cone beam computed tomographs were captured for each model to plan the positions of zygomatic implants. The hand-eye calibration technique was used to register the dynamic navigation system to the robotic spaces. A total of 16 zygomatic implants were placed, equally distributed between the anterior and the posterior parts of the zygoma. The placement of the implants (ZYGAN®, Southern Implants) was carried out using an active six-jointed robotic arm (UR3e, Universal Robots) guided by the dynamic navigation coordinate transformation matrix. The accuracy of the implant placement was assessed using EvaluNav and GeoMagicDesignX® software based on pre- and post-operative CBCT superimposition. Descriptive statistics for the implant deviations and Pearson's correlation analysis of these deviations to force feedback recorded by the robotic arm were conducted.

Results: The 3D deviations at the entry and exit points were 1.80 ± 0.96 mm and 2.80 ± 0.95 mm, respectively. The angular deviation was $1.74 \pm 0.92^\circ$. The overall registration time was 23.8 ± 7.0 min for each side of the model. Operative time excluding registration was 66.8 ± 8.8 min for each trajectory.

The exit point and angular deviations of the implants were positively correlated with the drilling force perpendicular to the long axis of the handpiece and negatively correlated with the drilling force parallel to the long axis of the handpiece.

Conclusion: The errors of the dynamic navigation-guided robotic placement of zygomatic implants were within the clinically acceptable limits. Further refinements are required to facilitate the clinical application of the tested integrated robotic-dynamic navigation system.

Clinical significance: Robotic placement of zygomatic implants has the potential to produce a highly predictable outcome irrespective of the operator's surgical experience or fatigue. The presented study paves the way for clinical applications.

1. Introduction

Zygomatic implants (ZIs), first reported by Branemark [1,2], are effective for the rehabilitation of atrophic maxillae [3,4]. A recent systematic review reported a high rate of surgical complications associated with the placement of ZIs which included perforation of the orbital floor, malposition of implants leading to early failure, and damage of the

infraorbital and zygomaticofacial nerves [5]. Postoperative pain, swelling and facial hematoma are among the most common complications due to the need for reflecting extensive mucoperiosteal flaps to expose the zygomatic bone during the surgery [5]. The flapless approach for dynamic navigation-guided placement of ZIs under local anaesthetic has been proven to be successful in reducing these complications [6,7]. Rehabilitation of these cases usually involves the placement of four ZIs

* Corresponding author.

E-mail address: Ashraf.Ayoub@glasgow.ac.uk (A.F. Ayoub).

<https://doi.org/10.1016/j.jdent.2024.105463>

Received 28 August 2024; Received in revised form 6 November 2024; Accepted 12 November 2024

Available online 13 November 2024

0300-5712/© 2024 The Author(s). Published by Elsevier Ltd. This is an open access article under the CC BY license (<http://creativecommons.org/licenses/by/4.0/>).

or two posterior ZIs with conventional anterior dental implants [8,9]. This depends on the availability of bone in three zones of the maxilla; the anterior, middle and posterior, zones I, II and III, respectively [10,11].

Planning ZIs involves the identification of the appropriate implant trajectories (i.e., pathways) based on the surrounding anatomical restrictions [12]. It is then followed by using a surgical guiding technique to ensure accurate execution of the plan [13].

The use of static guides, also termed surgical templates, is the most commonly used method when placing ZIs, but they have their limitations [14]. Errors associated with the initial versions of these templates have been reported [14]. Schirotti et al., proposed a flapless approach for ZI placement using static guides [15]. They reported the challenge in achieving the desired implant angulation [15,16]. J. Chow proposed a specially designed ZI drilling guide to supplement the conventional static surgical template [17]. It consisted of two metallic pieces that ensured a straight trajectory between the entry and exit points which enhanced the optimal implant positioning [17]. Bedrossian et al., highlighted the prevention and management of complications associated with ZI placement [18]. Jayanetti et al., suggested the use of double sleeves when the anatomy allows it (in ZAGA-3 and 4 cases) [19]. Rigo et al., advocated a fully guided ZI placement approach to simplify the conventional surgical procedure by using metallic surgical templates [20]. The availability of supporting bone is required for fixation of the template [20]. Gallo et al. showed that the differences in the accuracy between the anterior and posterior ZI and between the right and left sides were statically non-significant [21]. Further research is ongoing in relation to the refinement of these guides [22,23].

Watzinger et al., were among the first to attempt ZI placement guided by surgical navigation system [24]. Their study on cadavers showed 1.7 ± 1.3 mm deviations at the implant entry point and 1.3 ± 0.8 mm deviations at the exit point [24]. The ZI placement using dynamic navigation has been heavily investigated recently [25–27]. Due to the increased confidence in the refined dynamic navigation techniques, Bhalariao et al. demonstrated the successful flapless placement of ZI guided by dynamic navigation in a prospective clinical randomized trial [6,7]. González-Rueda et al. added the mixed-reality dimension using HoloLens glasses [28]. Optimising the registration of patient space and enhancing the drill calibration process are crucial to improve the accuracy of the placement of dental and zygomatic implants under dynamic navigation guidance [29,30].

It has been shown that dynamic navigation is dependent on the operator's manual dexterity and requires extensive training to maximise the visual-manual coordination [27,31]. These limitations inspired the development of the robotic placement of ZIs [32,33]. Shengchi, Cao et al. were among the first investigators of robotic systems for the placement of ZIs in vitro [32,33]. This was followed by Li, Deng et al., who tried the two-stage protocol in vitro and in a subsequent clinical investigation [34,35]. Their protocol involved the use of the semi-active Remebot® system to prepare the alveolar ridge in the first stage, followed by the manual insertion of the zygomatic drills into the prepared socket in the second stage. The robotic drilling of the zygomatic bone was then completed [34,36,37]. Implementing the HoloLens glasses to achieve a mixed-reality environment constitutes a novel ZI placement protocol using a "hybrid" robotic implant surgery [38].

Robotic technology proved to be successful in the placement of dental and ZIs [38–40]. It has the advantages of efficiency and precision, as well as allowing the flapless placement of dental implants, sinus lift procedure, and endodontic surgery [40–42]. Xu et al. evaluated active (Yekebot®), semi-active (Remebot®), and passive (DentRobot®) optically tracked commercial implant robotic systems [43]. They reported better accuracy of implant position with active and semi-active systems which required less human-robot interaction during surgery in comparison with the passive systems [43]. Passive and semi-active robotic systems require the operator to guide the robotic arm while entering and exiting the patient's mouth. Therefore, these steps took less time than with active robotic systems which require extensive

calibration-registration-verification processes that are time-consuming [43,44]. Studies on the accuracy of, Yomi®, reported higher errors in the placement of implants, both in vitro [45] and in a clinical series [46].

Yang et al., divided the robotic systems into 5 levels of autonomy; level 1 being robotic assistance (i.e., passive robotics such as DentRobot®, Cobot®, and Yomi® systems), level 2 being task autonomy (i.e., semi-active and active robotics such as Remebot® and Yekebot® systems), and levels 3 to 5 being the target for future development (conditional autonomy, high autonomy, and full automation which require the inclusion of artificial intelligence) [47]. Huang et al. promoted the use of a dual robotic arm system to overcome the obstructed field of vision of the tracking camera [48]. Tang et al. have also suggested the same concept [49]. The workflow for full arch rehabilitation with immediate dental implants is currently under consideration [50, 51].

In this project, we developed a task-autonomous active robotic system which is composed of a 6 degrees of freedom robotic arm (UR3e) and an optical dynamic navigation system (NaviDent®).

The aim of this study was the in vitro assessment of the feasibility and accuracy of the developed system for the dynamic navigation-guided robotic placement of ZIs.

2. Materials and methods

2.1. Materials

The robotic arm (UR3e; Universal Robots®, Odense, Denmark) was used to autonomously perform the implant osteotomy and placement of the ZIs. In addition to monitoring the positions of the drill tips in real-time, the dynamic navigation system (NaviDent®; ClaroNav Inc., Toronto, Canada) was integrated with the robotic software (on a laptop) to provide the coordinates of the entry and exit points of the planned ZIs. These coordinates were transmitted initially in static snapshots to calculate the transformation between the dynamic navigation system and the robotic arm. The real-time transmission of the coordinates was implemented throughout the implant placement procedure to maximise its accuracy. A 300 Mbps wireless N 4G LTE router (TL-MR6400; TP-Link technologies®, Shenzhen, China) was utilised to transmit the coordinates from the dynamic navigation system to the laptop controlling the robotic arm.

Six fiducial markers were placed in each plastic edentulous maxillary model (ZYG NM01 - D2 density; SelModels®, Barcelona, Spain) according to a previously optimised configuration [29]. The fiducial markers were 1.2 × 6 mm plate fixation screws (59-12106 - Leibinger Micro Plus System; Stryker Leibinger GmbH, Freiburg, Germany). The osteotomy cuts were carried out using short drills and a drill extension of the NobelReplace® kit (Nobel Biocare®, Zurich, Switzerland), in addition to the standard zygomatic osteotomy drills (Southern Implants®, Irene, RSA). ZYGAN implants (Southern Implants®, Irene, RSA) were used in the study. The implant engine (SI-95 230 - Implantmed®; W&H®, Bürmoos, Austria) and the implant contra-angle handpiece (WS-75; W&H®, Bürmoos, Austria) were connected to the end effector of the robotic arm via a custom-made 3D-printed connection that was made using Rigid 10K resin and a FormLabs 3D printer (Form 3B; FormLabs®, Somerville, USA). The same resin and 3D printer were used to construct a custom rigid connection between the edentulous maxillary models and the dental simulator (EWL 5190 Dental Simulation Unit; KaVo Electrotechnisches Werk GmbH, Leutkirch im Allgäu, Germany). Each model was also covered with a silicone mask to mimic the skin of the face (Silicone mask for simulated jaws non-latex; Wright Cottrell, Dundee, Scotland). The final system setup is shown in Fig. 1.

2.2. Planning the zygomatic implant trajectories

The study was carried out on eight commercially available plastic midface models that included the edentulous maxilla, the zygomatic

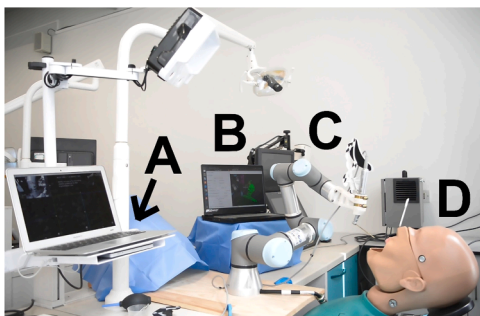


Fig. 1. The system setup for the robotic placement of zygomatic implants guided by dynamic navigation. (A): the dynamic navigation system. (B): the laptop controlling the robotic arm. (C): the robotic arm attached to a contra-angle implant handpiece and its tracker through a custom-made rigid connection. (D): The dental simulator carrying the plastic edentulous maxillary model with an attached jaw tracker. The coordinate transformation matrices are transferred between the optical tracking system and the robotic arm over a wireless connection router (not seen in this photo).

bones, the nose and the orbital cavities (Fig. 2). A set of radiopaque teeth (SR Vivo TAC/SR Ortho TAC; Ivoclar®, Zurich, Switzerland) was arranged in a prosthodontic laboratory to fit on the edentulous maxilla. A cone-beam computed tomography scan (CBCT) of the model with the radiopaque teeth fitted in place (model placed upside down) was obtained using the dental imaging unit (KaVo OP 3D Vision; KaVo Dental GmbH, Biberach, Germany). A Standard Tessellation Language (STL) file was derived from the CBCT DICOM image using InVesalius software (v.3.1.1). This STL file was then oriented according to the dental arch axes (i.e., midline and occlusal plane) using MeshMixer software (v.3.5.474). The soft tissue counterpart (i.e., the silicone layer) was segmented out of the resin using 3D Slicer software (v.5.1.0), and the result was saved as STL file for planning. Four ZIs were digitally planned according to the expected prosthetic rehabilitation and the anatomy-guided principles [52,53] (Fig. 2). The planning was achieved with the aid of an in-house developed STL library of the ZYGAN implants.

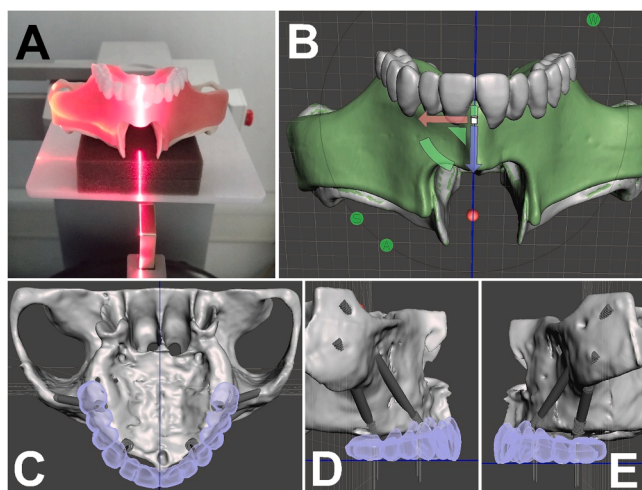


Fig. 2. The steps involved in creating a standardised plan for the zygomatic models. (A): A preoperative CBCT scan with the radio-opaque teeth fitted in place. (B): The initial orientation of the pre-operative model STL file in MeshMixer. (C-E): Appending implant STL files to the model STL after segmenting the soft tissue and the teeth in 3DSlicer to create the implant plan. Planning in STL mode allows precise control over the prosthodontic axis of the implant because the rotation and translation of any implant STL file can be easily restricted to one plane only, thus facilitating the control of implant depths in both alveolar and zygomatic regions while also observing anatomical and safety planning principles simultaneously.

Planning in STL mode allows precise control of implant depths in both alveolar and zygomatic regions while also observing anatomic, prosthetic, and safety planning principles simultaneously. Two implants were planned in each model; 50 mm long (ZAGA-1) anterior ZIs and 35–40 mm long (ZAGA-2) posterior ZIs [54]. Therefore, 16 ZIs were placed in 8 plastic models (two implants per model). The location of the two implants was similar in each two of the 8 plastic models. ZIs were placed in the right anterior and left anterior positions in two models, in the posterior right and left positions in two models, in the right anterior and posterior positions in two models, and in the left anterior and posterior positions in the last two models. The implant cones, specific to the dynamic navigation software, were digitally placed on the STL file of the planned implants, using the dynamic navigation software (NaviDent® v.3.0.3).

2.3. The drill calibration and registration procedures

A rigid connection was established between the implant handpiece and the end effector of the robotic arm. A single drill calibration protocol was implemented for the robotic osteotomy. The selection of the calibration drill (zygomatic spade drill with one drill extension) was based on our previous study which showed its higher precision with all planned points [30]. After this single drill calibration, the visual representation displayed by the navigation camera was used to determine its accuracy (the short green line on the NaviDent® screen - Fig. 3). This routine checking was independent of the registration between the patient space and the NaviDent® space.

Following drill calibration, the registration of the patient space and the NaviDent® space was carried out according to the manufacturer's instructions and based on the six fiducial markers of each model [29]. The accuracy of this registration was determined using the manufacturer-provided tracer tool.

A standard hand-eye calibration method was performed based on 15 robotic arm poses around the operative area to register the spatial relationship between the NaviDent® space and the robotic arm space [55]. The rigid fixation of the base of the robotic arm and the location of the plastic model was ensured prior to this registration step. In each of the 15 robotic poses, the sampling process captured the transformation matrix between the jaw tracker and the tip of the drill (as recorded in the dynamic navigation system) as well as the transformation matrix between the base of the robotic arm and the frame of reference of its end effector (as recorded in the robotic arm system). This information was transmitted wirelessly between the dynamic navigation system and the robotic arm system. The synchronised sampling allowed the calculation of the fixed spatial relationship between the base of the robotic arm and the jaw tracker of the navigation system and the fixed spatial relationship between the tip of the drill and the end effector of the robotic arm. In this way, the robotic arm could perform, within a given reach and safety restrictions, the planned procedure at any desired pose between the drill tip and the plastic model according to the entry and exit point coordinates of that particular implant trajectory.

The accuracy of this step was checked by commanding the programmed robotic arm to approach one of the implant entry points. This was monitored on the NaviDent® screen to confirm the satisfactory accuracy of coordinate match (Fig. 4). The registration of the NaviDent®-to-robotic spaces was then fine-tuned to have the highest accuracy at the exit point of the implant-planned trajectory. The fine-tuning step involved capturing more transformation matrix samples (~2100 samples over 3 sec) and re-applying the calculations for the two fixed spatial relationships as explained above.

The robotic control user interface, which was developed in-house, automatically adjusted for the differences in the length of the osteotomy drills and implants while keeping the single drill calibration information within the NaviDent® system.

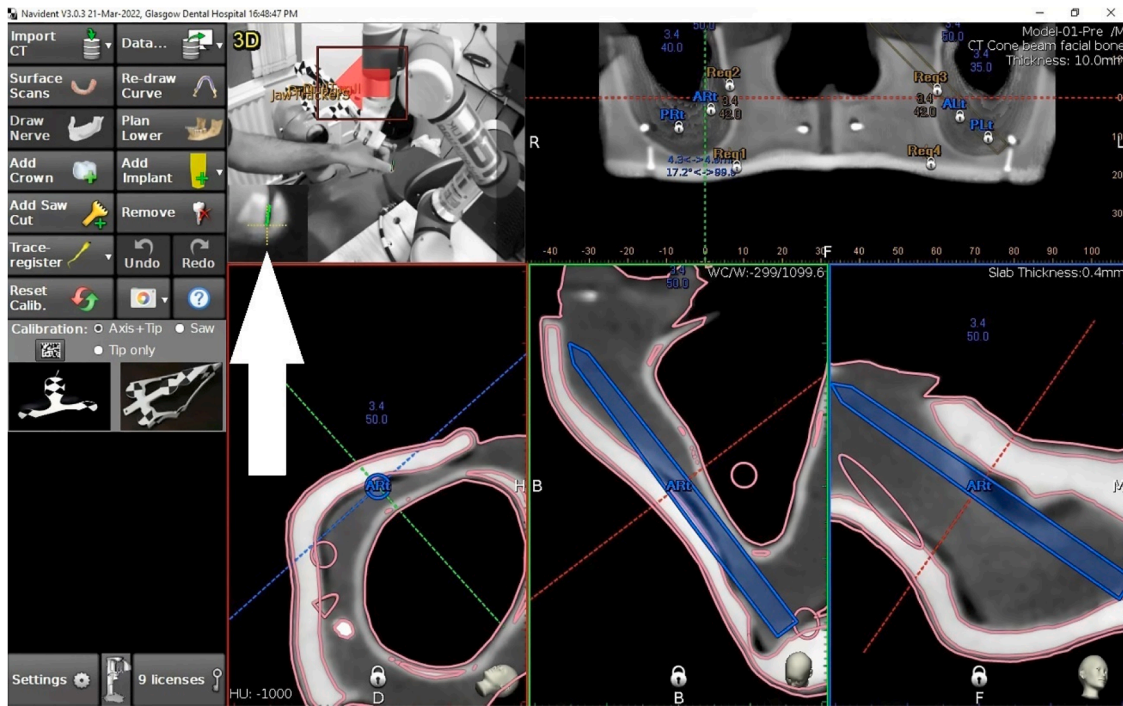


Fig. 3. The drill calibration accuracy check process for single drill calibration protocol.

The visual representation of the drill tip (as a short green line) is shown at the bottom left corner of the camera view (upward pointing white arrow). If this green line was deviated from the real drill tip seen in this view, the single drill calibration process was repeated to improve the accuracy of the calibration.

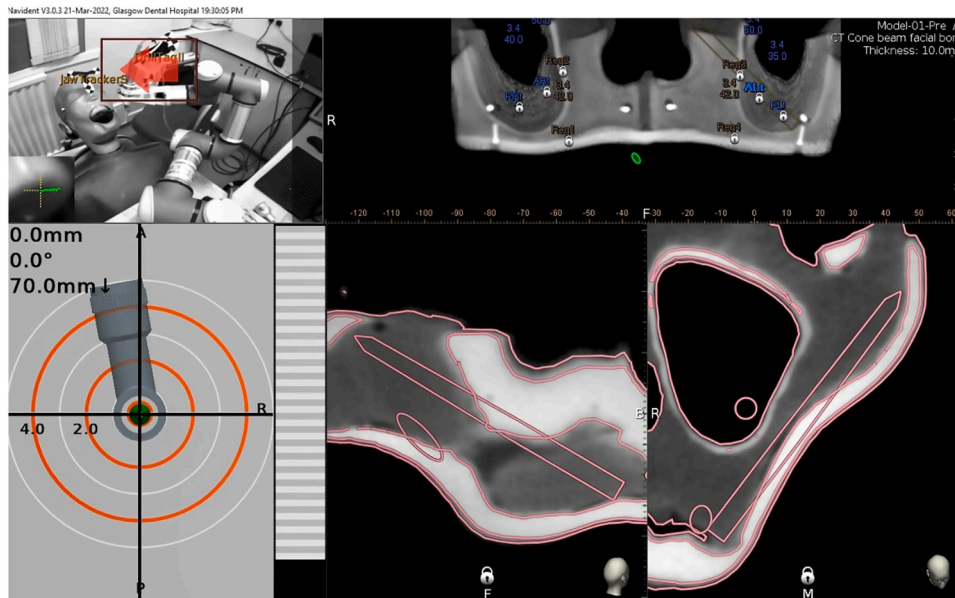


Fig. 4. The accuracy checking method for the hand-eye calibration process in the degree of matching the coordinates of the dynamic navigation system and the robotic arm space. In this specific example, the robotic arm was commanded to approach the entry point of the anterior left ZI at a safe distance of 20 mm after detaching the actual drill that was used for the drill calibration. The 70 mm depth displayed in the target view at the bottom left corner of the screen equals the length of the implant trajectory (50 mm) plus the safe distance (20 mm).

2.4. The drilling and implant placement procedures

After using a tissue punch to remove the silicone layer on the models overlying the implant entry locations, the following drilling steps were carried out according to the manufacturer's instructions : A speed of 2000 rpms for the short alveolar osteotomy drills, 1500 rpms for the stainless-steel zygomatic drills and the side-cutting drill, and 1000 rpms for the titanium zygomatic drills. The advancing speeds were 2 % (~0.5

mm/second) for the drilling and 4 % (~1.0 mm/second) for the implant insertion (Fig. 5). The stepwise drilling allowed the pre-planned trajectory of the osteotomy to be gradually achieved using a standard set of drills until the final placement of the ZI.

The real-time transmission of coordinates between the Navident® system and the robotic control software during the implant placement step ensured that the implant engine automatically stopped when the final desired depth was reached. The communication between the

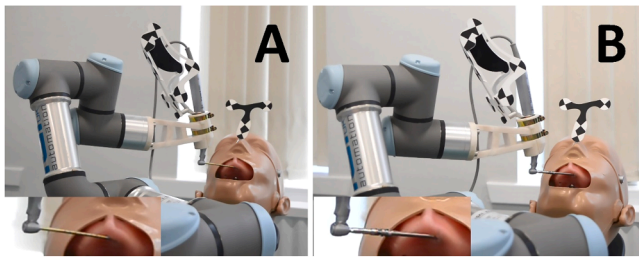


Fig. 5. Photographs showing the robotic arm in action. (A): The stage of implant osteotomy using a titanium zygomatic twist drill 2.7Φ. (B): The stage of zygomatic implant placement. The bottom left corners show magnified views of the operative area.

software of the robot-controlling laptop and the implant engine was established through an automated power switch-off hardware that disconnected the main power to the implant engine once it received the signal of reaching the final depth. The duration of each procedural step was recorded. The continuous streams of data from the standard force sensor integrated into the robotic arm (i.e., force feedback data) were captured in screen recordings throughout all the steps of the implant osteotomy.

The plastic models were re-scanned after placing the ZIs, the CBCT scans were imported into EvaluNav software for the assessment of their accuracy. The pre-operative and its corresponding post-operative CBCTs were superimposed using the fiducial markers and other landmarks that did not change due to the osteotomy or the implant placement. The quality of this superimposition was ensured according to the available features in the EvaluNav software. The EvaluNav software then detected the actual implant positions in the post-operative CBCT via the automated alignment function. MeshMixer (v.3.5.474) and MeshLab (v.2021.05) software were utilised to standardise the frame of reference of the implants. The X axis represented the mediolateral direction (along the occlusal plane), the Y axis represented the antero-posterior direction, and the Z axis represented the vertical direction (Fig. 6). The common frame of reference allowed the extraction of the coordinates of the planned and the placed implants using GeoMagic Design X® software (3D Systems, v.2020.0.3).

The 3D distance deviations between the planned position and the actual position of the ZIs were calculated according to the following equations:

$$3D \text{ distance deviation} = \sqrt{(\text{mediolateral deviation})^2 + (\text{anteroposterior deviation})^2 + (\text{vertical deviation})^2}$$

The 3D angular deviations were calculated with the equation:

$$3D \text{ angle} = \cos^{-1} \frac{X \text{ vector} + Y \text{ vector} + Z \text{ vector}}{(\text{planned ZI length}) * (\text{actual ZI length})}$$

where:

$$X \text{ vector} = (\text{planned ZI entry X} - \text{planned ZI exit X}) * (\text{actual ZI entry X} - \text{actual ZI exit X})$$

$$Y \text{ vector} = (\text{planned ZI entry Y} - \text{planned ZI exit Y}) * (\text{actual ZI entry Y} - \text{actual ZI exit Y})$$

$$Z \text{ vector} = (\text{planned ZI entry Z} - \text{planned ZI exit Z}) * (\text{actual ZI entry Z} - \text{actual ZI exit Z})$$

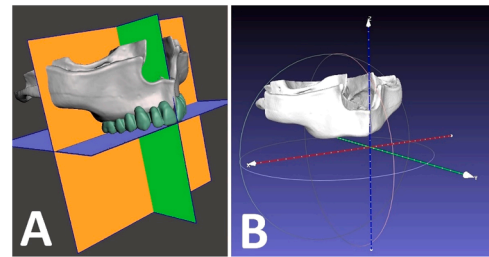


Fig. 6. The steps involved in creating a standardised frame of reference for the analysis of the zygomatic implant deviation directionality. (A): Identifying the planes of directionality in MeshMixer software based on the planned replacement dentition. (B): Aligning the point of origin of the standardised model in MeshLab software according to the previously identified plane representations. This was followed by removal of these planes as well as the replacement dentition. X axis represented the mediolateral direction (green plane movement in A), Y axis represented the coronal direction (orange plane movement in A), and Z represented the superior-inferior direction (blue plane movement in A). All pre- and post-operative STL files were brought to this standardised frame via the mesh superimposition function in MeshMixer prior to the deviation analysis.

The x, y, and z force vectors (in newtons) were extracted from the force recordings of 12 out of the 16 trajectories. Next, XY force vectors as well as 3D force vectors were calculated. The mean force during the drilling steps (D.Mean) as well as the maximum recorded force during the drilling steps (D.Max.) were also measured.

2.5. Statistical analysis

Sample size calculation was based on the angular deviations from the study of Cao et al. [33]. In that study, the zygomatic implants angular deviations were 2.07 ± 0.30 degrees for the manual dynamic navigation group and 1.52 ± 0.58 degrees for the robotic group. A pooled standard deviation of 0.532541 degrees was calculated using the formula $\sqrt{\frac{(n_1-1)s_1^2 + (n_2-1)s_2^2}{n_1 + n_2 - 2}}$, before input into the power calculation software (G*Power v.3.1.9.7). The other calculation settings were for an independent group comparison, with α set at 0.05 and sample power at 0.8. This resulted in a sample size of 16 zygomatic implants for any study group.

SPSS statistics (IBM SPSS, v.26) was used for the statistical analysis.

The Shapiro-Wilk normality test was applied. Correlation analysis between the generated forces during the implant osteotomy and placement steps and the measured deviations of the placed implants was conducted using SPSS software and expressed in terms of Pearson's correlation coefficient. GraphPad (Prism®, v.9) was used to create the graphical representations.

3. Results

The median deviations at the entry points of the implants were 0.31 mm, -0.05 mm, and -0.36 mm in the vertical, coronal and mediolateral directions, respectively. The median deviations at the exit points of the implants were -0.05 mm, -0.58 mm, and -0.38 mm in the vertical, coronal and mediolateral directions, respectively. The negative values represent deviations in the downward, backward and medial directions (Fig. 7). Considering the exit point of the placed implants; the upward,

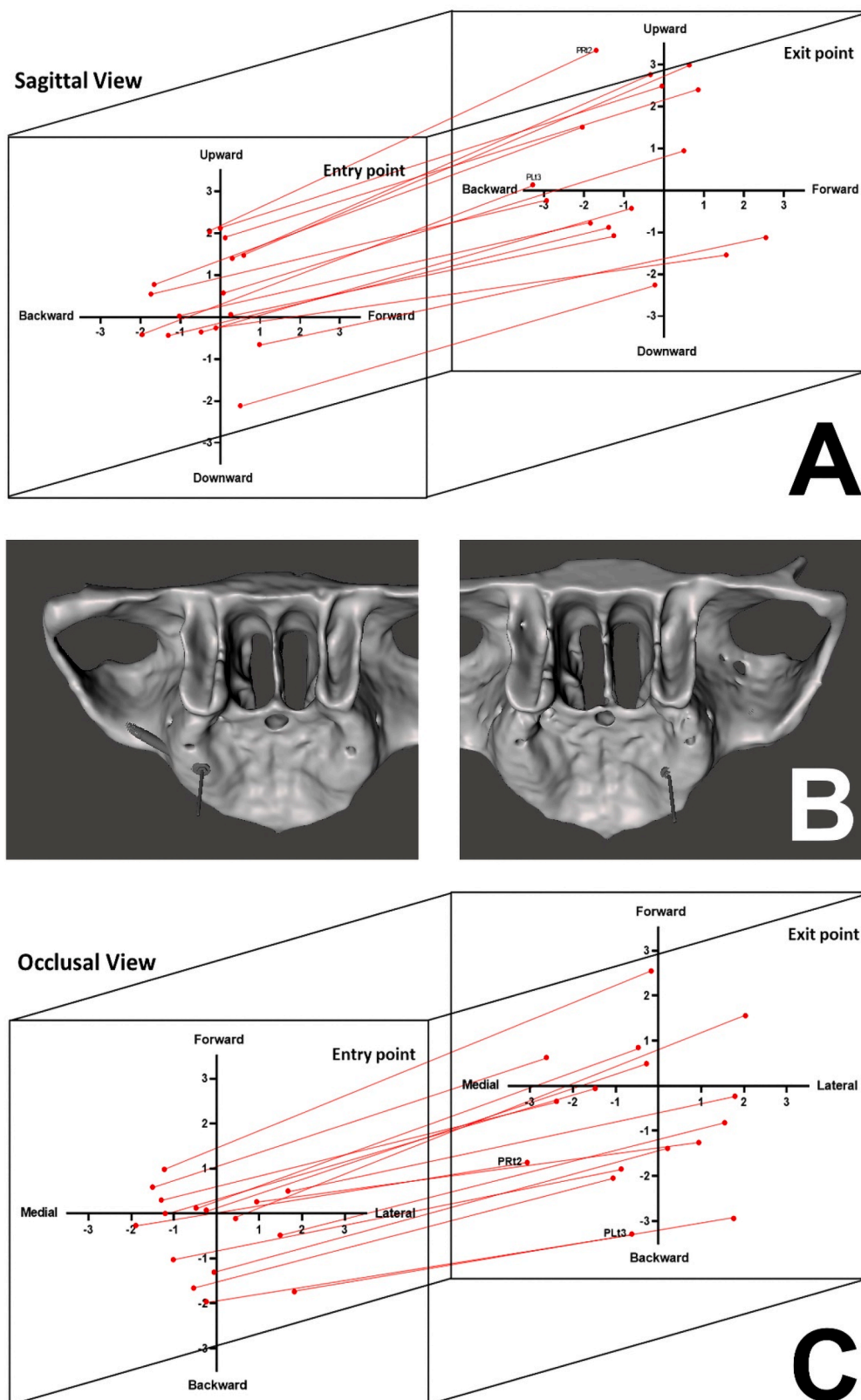


Fig. 7. (A): A sagittal 3D scatter diagram depicting the distribution of the ZI entry and exit point deviations in every direction except mediolaterally. The lines are connecting each entry point deviation to its corresponding exit point deviation so that the angular discrepancy can also be judged from this view. (B): 3D representations of the actual ZI positions of the most extreme exit point deviation cases; a posterior left ZI apex was deviated 3.29 mm backward, and a posterior right ZI apex in another model was deviated 3.35 mm upward and 3.07 mm medially. (C): An occlusal 3D scatter diagram to show the distribution of mediolateral deviations which had to be ignored from the sagittal view.

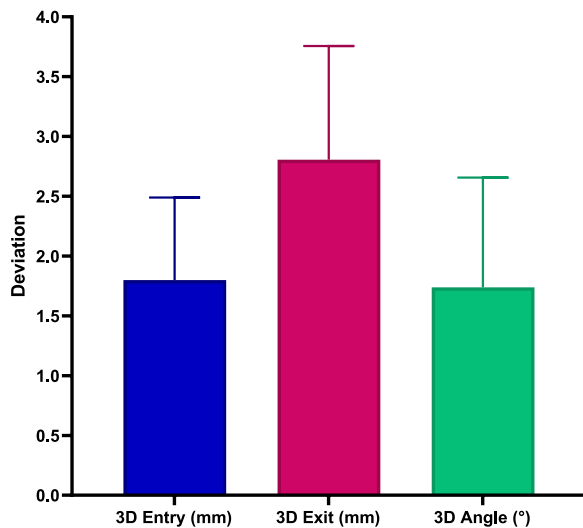


Fig. 8. A bar chart demonstrating the 3D deviation parameters that resulted from testing the study group (robotic implant drilling and placement). Number of values in each bar (n = 16). The error bars represent the standard deviations from the mean values.

medial, and backward deviation directions were of clinical importance due to the close proximity to the orbital floor and the infra-temporal fossa (Fig. 2: C-E). Out of the 16 ZIs; upward deviations of 2.07 mm (± 1.11 mm) were noted in 8 implants, backward deviations of -1.45 mm (± 1.06 mm) were detected in 11 implants, whereas medial deviations of -1.30 mm (± 1.04 mm) were detected in 10 implants. The only two apical deviations exceeding 3 mm were a posterior left ZI which had a 3.29 mm backward deviation and a posterior right ZI in another model which had a 3.35 mm upward and a 3.07 mm medial apical deviation. The apical deviations in both of these ZIs are of limited clinical significance (Fig. 7: B).

The mean (\pm SD) values of the 3D deviations of implant entry and exit points as well as the angular disparities are shown in Fig. 8. These were 1.80 ± 0.96 mm, 2.80 ± 0.95 mm, and 1.74 ± 0.92 degrees, respectively.

The overall registration time was 23.8 ± 7.0 min (mean \pm SD) for each side of a model. Operative time excluding registration was $66.8 \pm$

8.8 min for each trajectory.

The relationships between actual ZI deviations and the mean of drilling 3D forces are shown in Fig. 9. With the exception of the posterior right ZIs, it can be noted in the figure that higher drilling forces were generally associated with less deviations. However, upon subsequent application of correlation analysis, this association was found to be weak and not statistically significant (Table 1). On the other hand, when the component force vectors were considered, statistically significant positive correlations were noted between the ZI angular and exit point deviations and the y force vector whereas statistically negative correlations were noted with the x force vector (Table 1).

4. Discussion

In the current study, the wireless transfer of the NaviDent® generated transformation matrices had enabled the hand-eye calibration protocol of the robotic arm to be achieved. The NaviDent® software (v.3.0.3) has the facility of automated axis adjustment algorithm for the calibration of the length of every drill. Therefore, one drill calibration protocol was followed to achieve a reproducible robotic position throughout the drilling procedure. An important feature of the robotic system used in this study was the automatic switch-off facility once the required depth of the implant placement was reached. This was based on the real-time transmission of the coordinates of the drill tip during the implant placement procedure.

In addition to possible human-related errors [29,30], we agree that the deviation of robotic dental implant placement is dependent on specific characteristics of the surgical site [56]. This is in agreement with the study by Du et al. using the SinoPlan® robotic system to place electrodes in the skull which showed that the trajectory-skull angle has significantly influenced the placement radial error [57]. The similarity between the long zygomatic drills and the neurological electrodes supports the concept that anatomical variations influence the magnitude and the direction of the deviations of the robotic placement of implants [56,57]. In the current study, we recorded higher deviations associated with the planned posterior trajectories, particularly at the point of the entry to the zygomatic bone. This observation agrees with a recent *in vitro* study by González-Rueda et al., using dynamic navigation [28]. However, we do not agree that the free-hand technique produces higher ZI accuracy than the computerised methods which include static-, dynamic navigation-, and augmented reality- guided methods [28]. This is

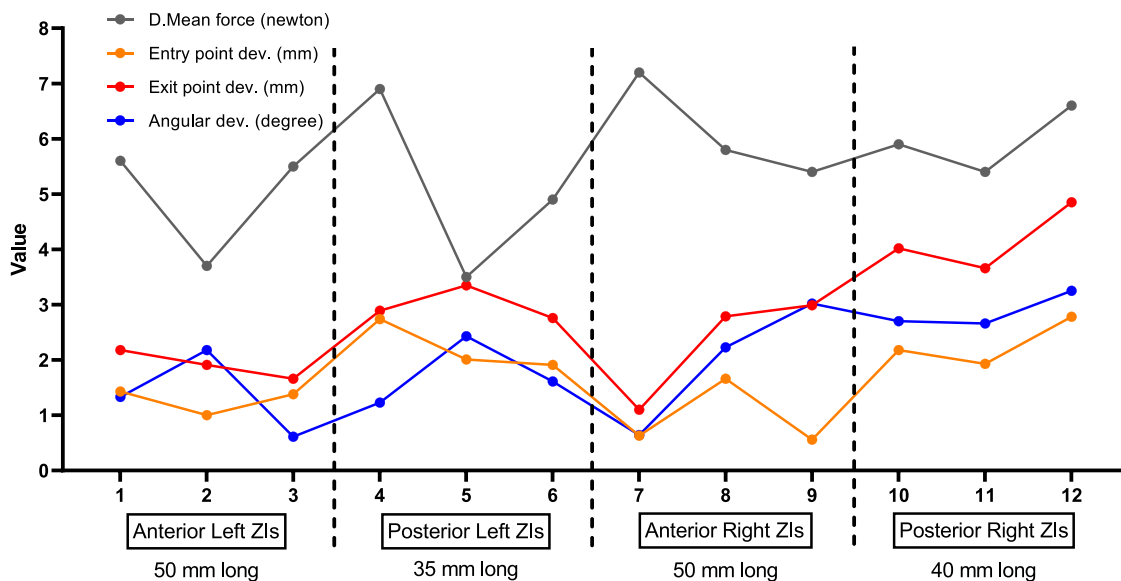
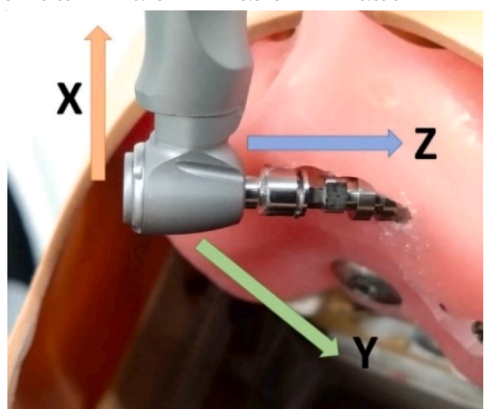


Fig. 9. A line graph showing the trajectory-specific relationships between the mean drilling force (D.Mean force) and the 3D actual implant deviations at its entry, exit as well as angular deviation from the planned trajectory.

Table 1

Pearson’s correlation coefficients to appreciate the associations between the force feedback recorded by the robotic arm (at the exit point of the trajectory) and the actual ZI deviations.

	SSpade	STwist	ZRound	ZSpade	ZTwist (2.7)	ZTwist (2.9)	ZSideC	ZCSink	ZImp.	D.Mean	D.Max
Correlation with Entry point 3D deviation											
X Force	-0.255	-0.458	-0.317	-0.313	-0.252	-0.520	-0.302	0.219	-0.154	-0.460	-0.441
Y Force	0.097	0.546	0.555	0.331	0.537	0.718 **	0.397	0.195	0.354	0.586 *	0.521
Z Force	-0.253	0.495	-0.560	-0.176	-0.256	-0.048	0.562	0.009	0.096	-0.099	-0.483
XY Force	-0.111	0.041	0.422	0.082	0.268	0.003	0.241	0.254	0.266	0.268	0.258
3D Force	-0.216	0.175	0.279	0.035	-0.095	-0.118	0.444	0.158	0.253	0.178	0.083
Correlation with Exit point 3D deviation											
X Force	-0.544	-0.845 **	-0.782 **	-0.647 *	0.008	-0.440	-0.560	0.026	-0.235	-0.832 **	-0.805 **
Y Force	-0.006	0.229	0.852 **	0.619 *	0.722 **	0.434	0.575	0.356	0.009	0.700 *	0.670 *
Z Force	-0.310	0.476	-0.122	-0.399	-0.568	-0.244	0.503	-0.033	-0.184	-0.216	-0.408
XY Force	-0.330	-0.407	0.527	0.151	0.536	0.006	0.242	0.291	-0.069	0.157	0.109
3D Force	-0.386	-0.304	0.496	0.032	-0.207	-0.180	0.446	0.132	-0.185	0.033	0.015
Correlation with Angular deviation											
X Force	-0.407	-0.761 **	-0.835 **	-0.731 **	0.276	-0.179	-0.531	-0.192	-0.305	-0.773 **	-0.750 **
Y Force	-0.016	-0.131	0.705 *	0.471	0.492	0.044	0.433	0.224	-0.184	0.443	0.421
Z Force	-0.263	0.152	0.207	-0.590 *	-0.782 **	-0.383	0.183	-0.160	-0.372	-0.431	-0.402
XY Force	-0.241	-0.546	0.322	-0.024	0.516	0.007	0.086	0.038	-0.283	-0.066	-0.109
3D Force	-0.281	-0.528	0.376	-0.165	-0.402	-0.211	0.183	-0.104	-0.466	-0.247	-0.160



Star symbols indicate statistically significant correlations in terms of p value: ** < 0.01, * < 0.05. SSpade = short spade drill; STwist = short twist drill 5.0Φ; ZRound = zygomatic round drill; ZSpade = zygomatic spade drill; ZTwist = zygomatic twist drill; ZSideC = zygomatic side-cutting drill; ZCSink = zygomatic counter-sink drill; ZImp. = zygomatic implant placement stage; D.Mean = mean drilling force; D.Max. = maximum drilling force. The photograph at the bottom of the table demonstrates the direction of the x, y and z force vectors: x is superior-inferior parallel to the long axis of the handpiece, y is mediolateral perpendicular to the long axis of the handpiece, and z is inward-outward (in relation to both the drill and the robotic end effector).

mainly because of the evidence pooled from other studies which contradicts this finding [26]. The length of the implant is another potential cause of the noted deviations in our study, but this requires further investigation [58]. Geometrically, with a zero translational movement at the entry point of the implant, a 5-degree angular deviation at the entry point would result in a 4.36 mm exit point deviation with a 50 mm long ZI, 3.05 mm deviation with a 35 mm long ZI, and 0.87 mm exit deviation with a 10 mm long conventional dental implant. Similarly, a 1.74-degree angular deviation at the entry point would result in a 1.52 mm exit point deviation with a 50 mm long ZI, 1.06 mm deviation with a 35 mm long ZI, and only 0.30 mm deviation with a 10 mm long conventional dental implant. However, dynamic navigation guided placement of ZIs tends to achieve accurate 3D positioning of the implant exit point over the translational errors at the entry point. In the current investigation using the robotic arm, changing the ZI implant length from 35 to 50 mm did not directly impact on the recorded implant deviations. A moderate negative correlation was noted between the e trajectory length and the deviation of the entry point of the implants (Pearson’s correlation coefficients: $r=-0.540$ with p value 0.031). The correlation was less with deviations of the exit point, and the angular deviations of the implants ($r=-0.373$ with p value of 0.155, and $r=-0.073$ with p value of 0.789, respectively).

In the current investigation, the mean ± SD values of the 3D deviations of implant entry and exit points as well as the angular deviations

were 1.80 ± 0.96 mm, 2.80 ± 0.95 mm, and 1.74 ± 0.92 degrees, respectively. The exit point deviations of the placed implants in the upward, backward and medial directions are of clinical importance due to the adjacent anatomical structures; mainly the orbital floor and the infra-temporal fossa. The distribution of these safety-related deviations in our study suggests that the current prototype is considered to be “clinically acceptable” according to the recent meta-analysis looking at dynamically-guided manual ZI placement which indicated an overall exit point accuracy of 2.95 mm with a confidence interval range of 1.66 to 4.24 mm [26]. Hung et al. considered a 2.15 ± 0.95 mm deviation at the exit point of ZI to be “safe” despite the fact that the maximum value reached 4 mm [25]. In a clinical study, Bhalarao et al. demonstrated the successful placement of zygomatic implants using dynamic navigation despite the 2 mm entry point, 5 mm exit point, and 6 degrees angular deviations, with no morbidities reported in their study [6,7]. Therefore, the results of our study are considered clinically acceptable with a recommendation for further refinements to improve the reproducibility and reduce the ZI placement errors [25,26]. Wang et al., reported ranges of 0.57–1.22 mm, 0.80–2.13 mm, and $0.91^\circ-1.58^\circ$, for entry point, exit point and angular deviation, respectively for zygomatic implant placement with robotic assistance. Their narrative review focused on the recent studies for robotic assisted implant placement with strict inclusion and exclusion criteria [59].

In a clinical study, a maximum error of 2.13 mm at the exit point with

the use of semi-active robotics for placement of ZIs was reported [34]. Interestingly, the maximum value of angular deviation also occurred with a right posterior ZI [34], which was similar to the maximum angular deviation of 3.25° that was associated with a posterior right ZI in our study. The authors believe that this common observation could be related to some mechanical limitation of the robotic arm joints while drilling in this position. It is less likely that the variation is related to the optical tracking system as the processes of tracking and registration were identical when drilling in the anterior right trajectory position.

Manual placement of ZIs guided by dynamic navigation took 8.68 ± 0.58 minutes after comprehensive training [27]. The surgical time with the current robotic prototype system was about eight-fold, 66.8 minutes (± 8.8 min). Therefore, further refinements of the dynamic navigation-guided robotic placement of ZIs should be directed towards the automation of the multiple registration, calibration and checking steps. To maximize the accuracy of the automated implant placement, we followed a strict calibration-registration-verification process which added ~ 15 min per trajectory. Although no time was required to re-calibrate every drill, there was a concern that the spatial relationship between the plastic model and the base of the robotic arm may undergo minor mechanical shifts during osteotomies. Therefore, frequent robotic arm pose reproducibility checks were carried out by approaching the exit point as if the final ZI twist drill was attached (i.e., these checks were carried out without attaching an actual drill to the handpiece). Based on these checks, the robotic registration had to be refined often. Similar “handpiece-in-air” testing was conducted before the ZI placement step, to check the functionality of the automated power switch-off hardware, which further added ~ 7 min per trajectory.

The advancing speed of the robotic arm drilling was set at a minimum rate of ~ 0.5 mm/second to avoid damage to the drills and the handpiece during the preparation of the implant site as well as to allow for the cutting of the model’s tough material. This minimum advancing speed setting has also added to the overall duration of the procedure. Likewise, the registration of the robotic arm was time-consuming (23.8 ± 7.0 min). Time saving may be considered one of the advantages of the passive robotic placement of dental implants [43]. To enhance the efficiency of the current system, future developments should focus on the automation of the initial registration steps, the incorporation of less frequent checks or the automation of these checks (e.g., by tracking three optical trackers simultaneously with automated trajectory refinement), and the utilisation of sharper drills which would encourage increased osteotomy advancing speed and possibly a reduced number of drilling steps.

Regarding the force feedback data, there was a tendency of higher deviations in ZI placement with the reduced mean drilling forces. The possible explanation of this finding is that the drills did not cut enough resin to allow the smooth placement of the implant which has contributed to the noted deviations.

The observed correlations with the component force vectors indicate that high resistance forces perpendicular to the long axis of the contra-angle handpiece (i.e., y force vector) were associated with more deviations of the placed implant. On the other hand, the resistance forces which were parallel to the long axis of the handpiece, as seen in the x force vector, were associated with less deviations, and may have arisen from the resistance encountered during the cutting of the resin. These associations can be most beneficial at the stage of drilling with the round zygomatic drill. It is expected that a low value of the x force vector and a high value of the y force vector would result in more errors in the implant placement.

It is important to highlight that the drilling forces were recorded at the end effector of the robotic arm rather than the cutting edge of the drill itself. Advanced force sensors are required to allow a more comprehensive exploration of the relationship between the generated cutting force and the deviations of the implant placement. These sensors would be expected to improve the overall safety of the system. Sharma et al., suggested the use of flexible drilling with a steering cannula to

reduce the stress and strain during the simulated spinal fixation procedure [60]. Hard-tissue lasers could be a useful alternative for bone cutting to reduce the exerted forces needed for the robotic placement of ZIs.

In summary, results presented in this study are encouraging, the main limitations that should be addressed before progressing to clinical applications are related to the high technical and time demands of the procedure. The technical steps should be further simplified and the overall accuracy improved before the developed system is ready for clinical use.

5. Conclusions

The current prototype integrated system showed promising results for dynamic navigation-guided placement of zygomatic implants using a six-jointed robotic arm. The resulting 3D deviations were 1.80 ± 0.96 mm, 2.80 ± 0.95 mm, and 1.74 ± 0.92 degrees for the entry point, exit point and angular deviation of the ZIs, respectively. The clinically-relevant exit point deviations were 2.07 ± 1.11 mm in the upward direction, 1.45 ± 1.06 mm in the backward direction, and 1.30 ± 1.04 mm in the medial direction. The overall registration time was 23.8 ± 7.0 min while the operative time excluding registration was 66.8 ± 8.8 min for each trajectory.

Further suggested improvements include the automation of procedural steps to reduce technical difficulties and time demands. The inclusion of force and torque sensors would be desirable to circumvent the anatomical variations which are encountered along the drilling trajectory.

List of Abbreviations

ZI, Zygomatic Implant
 RSA, Republic of South Africa
 USA, United States of America
 CBCT, Cone-Beam Computed Tomography
 STL, Standard Tessellation Language
 ZAGA, Zygoma anatomy guided approach
 SD, Standard Deviation
 +ve, Positive
 D. Mean, Mean drilling force
 D. Max., Maximum drilling force

CRediT authorship contribution statement

Mohammed Y. Al-Jarsha: Conceptualization, Methodology, Investigation, Data curation, Formal analysis, Writing – original draft.
Yufeng Diao: Methodology, Investigation, Writing – review & editing.
Guodong Zhao: Methodology, Supervision.
Muhammad A. Imran: Methodology, Supervision.
Ashraf F. Ayoub: Methodology, Supervision, Writing – review & editing.
Douglas P. Robertson: Methodology, Supervision, Writing – review & editing.
Kurt B. Naudi: Methodology, Supervision, Writing – review & editing.

Declaration of competing interest

The authors declare that they have no known competing financial interests or personal relationships that could have appeared to influence the work reported in this paper.

Acknowledgements

The authors would like to acknowledge the help of the following colleagues for their support:

Mary-Anne Ferguson (preclinical skills laboratory manager), and Linda McMichael (clinical support worker) for their help in facilitating access to the lab.

Lyndsey Johnston (territory manager at Nobel Biocare®) for her help in providing small models, conventional implant dummies, and an

implant drilling kit during the initial stages of the robotic prototype drilling tests.

Robert Pounds and Arish Qazi (NaviDent® support and software development) for their continued technical support during the development of the Dynamic-robotic system.

Stephen Dunn (lecturer) for his help with the 3D printing.

Graham MacDonald (prosthodontics laboratory manager) for arranging the radio-opaque teeth (in a wax-up) to standard zygomatic implant plan.

Amy Wylie (clinical dentistry section administrator) for her help in purchasing materials required for the experiment.

David Carrigan (electrician) for providing his help on maintenance issues during the experiment.

Sean Bunton for his help in the wood workshop for the robust foundation of the robotic arm.

Zishaan Iqbal, Emma MacDonald, Nisreen Jalal, and Diane McCallum (diagnostic dental radiographers) for their help in obtaining the pre-and post-operative CBCT scans.

References

- P.I. Brånemark, K. Gröndahl, L.O. Öhrnell, P. Nilsson, B. Petruson, B. Svensson, P. Engstrand, U. Nannmark, Zygoma fixture in the management of advanced atrophy of the maxilla: technique and long-term results, *Scand. J. Plast. Reconstr. Surg. Hand Surg.* 38 (2) (2004) 70–85, <https://doi.org/10.1080/02844310310023918>.
- J. Chow, *Zygomatic Implants: Optimization and Innovation*, Springer International Publishing, 2020 3030292649. ISBN: 9783030292645.
- G. Pellegrino, F. Basile, D. Relics, A. Ferri, F. Grande, A. Tarsitano, C. Marchetti, Computer-aided rehabilitation supported by zygomatic implants: a cohort study comparing atrophic with oncologic patients after five years of follow-up, *J. Clin. Med.* 9 (10) (2020) 3254, <https://doi.org/10.3390/jcm9103254>.
- T. Testori, T. Clauser, A. Rapani, Z. Artzi, G. Avila-Ortiz, S. Barootchi, E. Bressan, M. Chiapasco, L. Cordaro, A. Decker, L. De Stavola, D.A. Di Stefano, P. Felice, F. Fontana, M.G. Grusovin, O.T. Jensen, B.T. Le, T. Lombardi, C. Misch, M. Pikos, R. Pistilli, M. Ronda, M.H. Saleh, D. Schwarz-Arad, M. Simion, S. Taschieri, M. Toffler, T.F. Tozum, P. Valentini, R. Vinci, S.S. Wallace, H.L. Wang, S.C. Wen, S. Yin, G. Zucchelli, F. Zuffetti, C. Stacchi, Indications for implant-supported rehabilitation of the posterior atrophic maxilla: a multidisciplinary consensus among experts in the field utilising the modified Delphi method, *Int. J. Oral Implantol. (Berl)* 17 (1) (2024) 89–100.
- P.W. Kämmerer, S. Fan, C. Aparicio, E. Bedrossian, R. Davó, D. Morton, G. M. Raghoebar, S. Zarrine, B. Al-Nawas, Evaluation of surgical techniques in survival rate and complications of zygomatic implants for the rehabilitation of the atrophic edentulous maxilla: a systematic review, *Int. J. Implant Dent.* 9 (1) (2023) 11, <https://doi.org/10.1186/s40729-023-00478-y>.
- A. Bhalerao, M. Marimuthu, A. Wahab, A. Ayoub, Dynamic navigation for zygomatic implant placement: a randomized clinical study comparing the flapless versus the conventional approach, *J. Dent.* 130 (2023) 104436, <https://doi.org/10.1016/j.jdent.2023.104436>.
- A. Bhalerao, M. Marimuthu, A. Wahab, A. Ayoub, The clinical evaluation of the dynamically navigated flapless placement of zygomatic implants: a randomized controlled trial, *Int. J. Oral Maxillofac. Implants* 39 (1) (2024) 40–49, <https://doi.org/10.11607/jomi.10443>.
- K.G. Varghese, N. Gandhi, N. Kurian, A.Y. Daniel, K. Dhawan, M. Joseph, M. G. Varghese, Rehabilitation of the severely resorbed maxilla by using quad zygomatic implant-supported prostheses: a systematic review and meta-analysis, *J. Prosthet. Dent.* 130 (4) (2021) 543–552, <https://doi.org/10.1016/j.prosdent.2021.11.007>.
- K. Wadde, S. Kokitkar, L. Venkatakrishnan, S. Ranganath, S. Khaire, Comparative evaluation of sinus complication and survival rates of quad zygoma versus Bizygoma in combination with two regular implants in atrophic maxilla: a systematic review and meta-analysis, *J. Maxillofac. Oral Surg.* 23 (3) (2024) 710–718, <https://doi.org/10.1007/s12663-024-02136-1>.
- C. Aparicio, C. Manresa, K. Francisco, P. Claros, J. Aláñez, O. González-Martín, T. Albrektsson, Zygomatic implants: indications, techniques and outcomes, and the zygomatic success code, *Periodontol.* 2000 66 (1) (2014) 41–58, <https://doi.org/10.1111/prd.12038>.
- A.A. Aalam, A. Krivitsky-Aalam, G.M. Kurtzman, L. Mahesh, The severely atrophic maxilla: decision making with zygomatic and pterygoid dental implants, *J. Oral Biol. Craniofac. Res.* 13 (2) (2023) 202–206, <https://doi.org/10.1016/j.jobcr.2023.01.008>.
- C. Aparicio, W.D. Polido, J. Chow, L. David, R. Davo, E.J. De Moraes, A. Fibishenko, M. Ando, G. McLellan, C. Nicolopoulos, M.A. Pikos, H. Zarrinkelk, T. J. Balsli, M. Penarrocha, Identification of the pathway and appropriate use of four zygomatic implants in the atrophic maxilla: a cross-sectional study, *Int. J. Oral Maxillofac. Implants* 36 (4) (2021) 807–817, <https://doi.org/10.11607/jomi.8603>.
- C. Aparicio, W.D. Polido, J. Chow, R. Davó, B. Al-Nawas, Round and flat zygomatic implants: effectiveness after a 1-year follow-up non-interventional study, *Int. J. Implant Dent.* 8 (1) (2022) 13, <https://doi.org/10.1186/s40729-022-00412-8>.
- B.R. Chrcanovic, D.R. Oliveira, A.L. Custódio, Accuracy evaluation of computed tomography-derived stereolithographic surgical guides in zygomatic implant placement in human cadavers, *J. Oral Implantol.* 36 (5) (2010) 345–355, <https://doi.org/10.1563/aid-joi-d-09-00074>.
- G. Schirolli, F. Angiero, A. Silvestrini-Biavati, S. Benedicenti, Zygomatic implant placement with flapless computer-guided surgery: a proposed clinical protocol, *J. Oral Maxillofac. Surg.* 69 (12) (2011) 2979–2989, <https://doi.org/10.1016/j.joms.2011.03.050>.
- G. Schirolli, F. Angiero, A. Zangerl, S. Benedicenti, F. Ferrante, G. Widmann, Accuracy of a flapless protocol for computer-guided zygomatic implant placement in human cadavers: expectations and reality, *Int. J. Med. Robot. Comput. Assist. Surg.* 12 (1) (2016) 102–108, <https://doi.org/10.1002/rcs.1646>.
- J. Chow, A novel device for template-guided surgery of the zygomatic implants, *Int. J. Oral Maxillofac. Surg.* 45 (10) (2016) 1253–1255, <https://doi.org/10.1016/j.jiom.2016.06.007>.
- E. Bedrossian, Zygomatic implants operative consideration to minimize technical errors, complications, and their management, *Atlas Oral Maxillofac. Surg. Clin. North Am.* 29 (2) (2021) 277–289, <https://doi.org/10.1016/j.cxom.2021.04.005>.
- J. Jayanetti, K. Shah, D. Chao, C. Drago, Double sleeve guided placement of quadruple zygomatic implants for rehabilitation of a patient with ectodermal dysplasia: a clinical report, *J. Prosthet. Dent.* 129 (6) (2021) 824–830, <https://doi.org/10.1016/j.prosdent.2021.09.008>.
- L. Rigo, J. Tolardo, E. Giammarinaro, U. Covani, G. Caso, Fully guided zygomatic implant surgery, *J. Craniofac. Surg.* 32 (8) (2021) 2867–2872, <https://doi.org/10.1097/scs.00000000000008005>.
- F. Gallo, F. Zingari, A. Bolzoni, S. Barone, A. Giudice, Accuracy of zygomatic implant placement using a full digital planning and custom-made bone-supported guide: a retrospective observational cohort study, *Dent. J. (Basel)* 11 (5) (2023) 123, <https://doi.org/10.3390/dj11050123>.
- F. Hernández-Alfaro, J. Bertos-Quílez, A. Valls-Ontañón, D. Paternostro-Betancourt, F. Pindaros-Georgios, G.M. Ragucci, Three-dimensional evaluation of the accuracy of zygomatic implant placement through an in-house fully guided approach, *Int. J. Oral Maxillofac. Implants* 38 (4) (2023) 747–756, <https://doi.org/10.11607/jomi.10045>.
- Y. Mao, X. Li, Q. Wang, J. Zhang, Application of titanium 3D-printed double-sleeve guide for zygomatic implants: a technique report, *J. Prosthodont.* 32 (8) (2023) 752–756, <https://doi.org/10.1111/jopr.13724>.
- F. Watzinger, W. Birkfellner, F. Wanschitz, F. Ziya, A. Wagner, J. Kremser, F. Kainberger, K. Huber, H. Bergmann, R. Ewers, Placement of endosteal implants in the zygoma after maxillectomy: a Cadaver study using surgical navigation, *Plast. Reconstr. Surg.* 107 (3) (2001) 659–667, <https://doi.org/10.1097/00006534-200103000-00003>.
- K.F. Hung, F. Wang, H.W. Wang, W.J. Zhou, W. Huang, Y.Q. Wu, Accuracy of a real-time surgical navigation system for the placement of quad zygomatic implants in the severe atrophic maxilla: a pilot clinical study, *Clin. Implant Dent. Relat. Res.* 19 (3) (2017) 458–465, <https://doi.org/10.1111/cid.12475>.
- S. Fan, G. Sáenz-Ravello, L. Diaz, Y. Wu, R. Davó, F. Wang, M. Magic, B. Al-Nawas, P.W. Kämmerer, The accuracy of zygomatic implant placement assisted by dynamic computer-aided surgery: a systematic review and meta-analysis, *J. Clin. Med.* 12 (16) (2023) 5418, <https://doi.org/10.3390/jcm12165418>.
- W. Wang, M. Zhuang, B. Tao, F. Wang, Y. Wu, Learning curve of dynamic navigation-assisted zygomatic implant surgery: an in vitro study, *J. Prosthet. Dent.* 132 (1) (2024), <https://doi.org/10.1016/j.prosdent.2024.03.037>, 178.e1-178.e12.
- J.R. González-Rueda, A. Galparsoro-Catalán, V.M. de Paz-Hermoso, E. Riad-Deglow, Á. Zubizarreta-Macho, J. Pato-Mourelo, S. Hernández-Montero, J. Montero-Martín, Accuracy of zygomatic dental implant placement using computer-aided static and dynamic navigation systems compared with a mixed reality appliance. An in vitro study, *J. Clin. Exp. Dent.* 15 (12) (2023) e1035–e1044, <https://doi.org/10.4317/jced.61097>.
- M.Y. Al-Jarsha, O. Almezayad, N. Alotaibi, K.B. Naudi, D.P. Robertson, A.F. Ayoub, The accuracy of intraoral registration for dynamic surgical navigation in the edentulous maxilla, *Int. J. Oral Maxillofac. Implants* 39 (3) (2024) 21–46, <https://doi.org/10.11607/jomi.10531>.
- M.Y. Al-Jarsha, A.F. Ayoub, M.M. Almgran, C.H. Liu, D.P. Robertson, K.B. Naudi, The precision of drill calibration for dynamic navigation, *J. Dent.* 146 (2024) 105032, <https://doi.org/10.1016/j.jdent.2024.105032>.
- Z. Xu, L. Zhou, M. Zheng, Y. Lin, W. Huang, J. Chen, Y. Li, D. Wu, The effect of implant surgery experience on the learning curve of a dynamic navigation system: an in vitro study, *BMC Oral Health* 23 (1) (2023) 89, <https://doi.org/10.1186/s12903-023-02792-8>.
- F. Shengchi, C. Zhenggang, Q. Chunxia, W. Feng, H. Wei, C. Xiaojun, W. Yiqun, The accuracy of surgical automatic robotic assisted implants placement in edentulous maxilla—an in vitro study, *Clin. Oral Implants Res.* 29 (S17) (2018), <https://doi.org/10.1111/clr.16813358>, 283-283.
- Z. Cao, C. Qin, S. Fan, D. Yu, Y. Wu, J. Qin, X. Chen, Pilot study of a surgical robot system for zygomatic implant placement, *Med. Eng. Phys.* 75 (2020) 72–78, <https://doi.org/10.1016/j.medengphy.2019.07.020>.
- H. Deng, J. Wang, L. Liu, Y. Li, Feasibility and accuracy of a task-autonomous robot for zygomatic implant placement, *J. Prosthet. Dent.* (2023) 00710–00712, <https://doi.org/10.1016/j.prosdent.2023.10.029>, S0022-3913(23).
- C. Li, M. Wang, H. Deng, S. Li, X. Fang, Y. Liang, X. Ma, Y. Zhang, Y. Li, Autonomous robotic surgery for zygomatic implant placement and immediately loaded implant-supported full-arch prosthesis: a preliminary research, *Int. J. Implant Dent.* 9 (1) (2023) 12, <https://doi.org/10.1186/s40729-023-00474-2>.

- [36] H. Deng, H. Bian, Y. Liang, J. Cao, Y. Sun, Y. Li, Semi-autonomous two-stage dental robotic technique for zygomatic implants: an in vitro study, *J. Dent.* 138 (2023) 104687, <https://doi.org/10.1016/j.jdent.2023.104687>.
- [37] H. Deng, H. Bian, C. Li, Y. Li, Autonomous dental robotic surgery for zygomatic implants: A two-stage technique, *J. Prosthet. Dent.* (2023), <https://doi.org/10.1016/j.prosdent.2023.05.033>. S0022-3913(23)00408-0.
- [38] X. Fan, Y. Feng, B. Tao, Y. Shen, Y. Wu, X. Chen, A hybrid robotic system for zygomatic implant placement based on mixed reality navigation, *Comput. Methods Programs Biomed.* 249 (2024) 108156, <https://doi.org/10.1016/j.cmpb.2024.108156>.
- [39] M. Olivetto, J. Bettoni, S. Testelin, M. Lefranc, Zygomatic implant placement using a robot-assisted flapless protocol: proof of concept, *Int. J. Oral Maxillofac. Surg.* 52 (6) (2023) 710–715, <https://doi.org/10.1016/j.ijom.2022.12.002>.
- [40] Y.N. Tian, B.X. Li, H. Zhang, L. Jin, [Development of dental robot implantation technology], *Zhonghua Kou Qiang Yi Xue Za Zhi* 58 (12) (2023) 1300–1306, <https://doi.org/10.3760/cma.j.cn112144-20230908-00148>.
- [41] X. Su, G. Wang, B. Zhao, X. Wang, Maxillary sinus floor elevation for implant placement assisted by an autonomous dental implant robotic system: a clinical report, *J. Prosthet. Dent.* (2024) 00241–00245, <https://doi.org/10.1016/j.prosdent.2024.03.044>. S0022-3913(24).
- [42] C. Liu, X. Liu, X. Wang, Y. Liu, Y. Bai, S. Bai, Y. Zhao, Endodontic microsurgery with an autonomous robotic system: a clinical report, *J. Endod.* 50 (6) (2024) 859–864, <https://doi.org/10.1016/j.joen.2024.02.005>.
- [43] Z. Xu, Y. Xiao, L. Zhou, Y. Lin, E. Su, J. Chen, D. Wu, Accuracy and efficiency of robotic dental implant surgery with different human-robot interactions: an in vitro study, *J. Dent.* 137 (2023) 104642, <https://doi.org/10.1016/j.jdent.2023.104642>.
- [44] S.L. Bolding, U.N. Reebye, Accuracy of haptic robotic guidance of dental implant surgery for completely edentulous arches, *J. Prosthet. Dent.* 128 (4) (2021) 639–647, <https://doi.org/10.1016/j.prosdent.2020.12.048>.
- [45] P.S. Mozer, A. Guentsch, An in vitro analysis of the accuracy of static and robot-assisted implant surgery, *Clin. Oral Implants Res.* 35 (5) (2024) 487–497, <https://doi.org/10.1111/clr.14233>.
- [46] J.M. Neugarten, Accuracy and precision of haptic robotic-guided implant surgery in a large consecutive series, *Int. J. Oral Maxillofac. Implants* 39 (1) (2024) 99–106, <https://doi.org/10.11607/jomi.10468>.
- [47] G.Z. Yang, J. Cambias, K. Cleary, E. Daimler, J. Drake, P.E. Dupont, N. Hata, P. Kazanzides, S. Martel, R.V. Patel, V.J. Santos, R.H. Taylor, Medical robotics-Regulatory, ethical, and legal considerations for increasing levels of autonomy, *Sci. Robot.* 2 (4) (2017) eaam8638, <https://doi.org/10.1126/scirobotics.aam8638>.
- [48] L. Huang, L. Liu, S. Yang, P. Khadka, S. Zhang, Evaluation of the accuracy of implant placement by using implant positional guide versus freehand: a prospective clinical study, *Int. J. Implant Dent.* 9 (1) (2023) 45, <https://doi.org/10.1186/s40729-023-00512-z>.
- [49] G. Tang, S. Liu, M. Sun, Y. Wang, W. Zhu, D. Wang, X. Li, H. Wu, S. Men, L. Zhang, C. Feng, Y. Wang, Y. Ding, High-precision all-in-one dual robotic arm strategy in oral implant surgery, *BDJ Open* 10 (1) (2024) 43, <https://doi.org/10.1038/s41405-024-00231-6>.
- [50] W. Wang, X. Li, C. Yao, B. Zhao, Robotic dental implant placement workflow for edentulous jaws, *J. Prosthet. Dent.* (2024), <https://doi.org/10.1016/j.prosdent.2024.04.030>. S0022-3913(24)00350-0.
- [51] Q. Shu, D. Chen, X. Wang, Q. Liu, Y. Ge, Y. Su, Accuracy of flapless surgery using an autonomous robotic system in full-arch immediate implant restoration: a case series, *J. Dent.* 145 (2024) 105017, <https://doi.org/10.1016/j.jdent.2024.105017>.
- [52] C. Aparicio, R. López-Pfriz, M. Peñarrocha, Preoperative evaluation and treatment planning. zygomatic implant critical zone (ZICZ) location, *Atlas Oral Maxillofac. Surg. Clin. North Am.* 29 (2) (2021) 185–202, <https://doi.org/10.1016/j.cxom.2021.05.003>.
- [53] C. Aparicio, W.D. Polido, H.M. Zarrinkelk, The Zygoma anatomy-guided approach for placement of zygomatic implants, *Atlas Oral Maxillofac. Surg. Clin. North Am.* 29 (2) (2021) 203–231, <https://doi.org/10.1016/j.cxom.2021.05.004>.
- [54] C. Aparicio, A proposed classification for zygomatic implant patient based on the zygoma anatomy guided approach (ZAGA): a cross-sectional survey, *Eur. J. Oral Implantol.* 4 (3) (2011) 269–275.
- [55] Z. Yan, Q. Tang, F. Wang, R. Guo, X. Wu, Q. Liu. The Dental Implant Robot System Based on Binocular Vision, 2023, *IEEE*, 2023, pp. 283–287, <https://doi.org/10.1109/ICRCV59470.2023.10329201>.
- [56] P. Li, J. Chen, A. Li, K. Luo, S. Xu, S. Yang, Accuracy of autonomous robotic surgery for dental implant placement in fully edentulous patients: a retrospective case series study, *Clin. Oral Implants Res.* 34 (12) (2023) 1428–1437, <https://doi.org/10.1111/clr.14188>.
- [57] C. Du, L. Wang, J. Yan, G. Li, Y. Wu, G. Zhao, D. Cui, W. Jin, S. Yin, The association between trajectory-skull angle and accuracy of stereoelectroencephalography electrode implantation in drug-resistant epilepsy, *World Neurosurg.* 184 (2024) e408–e416, <https://doi.org/10.1016/j.wneu.2024.01.139>.
- [58] Y. Wang, S. Yu, Y. Wang, Y. Feng, Q. Yan, Y. Zhang, Effect of implant shape and length on the accuracy of robot-assisted immediate implant surgery: an in vitro study, *Clin. Oral Implants Res.* 35 (3) (2024) 350–357, <https://doi.org/10.1111/clr.14232>.
- [59] M. Wang, F. Liu, X. Zhao, Y. Wu, Robot-assisted surgery for dental implant placement: a narrative review, *J. Dent.* 146 (2024) 105034, <https://doi.org/10.1016/j.jdent.2024.105034>.
- [60] S. Sharma, Y. Sun, J. Bonyun, M. Khadem, J. Amadio, A.H. Eskandari, F. Alambeigi, A biomechanics-aware robot-assisted steerable drilling framework for minimally invasive spinal fixation procedures, *IEEE Trans. Biomed. Eng.* 71 (6) (2024) 1810–1819, <https://doi.org/10.1109/TBME.2024.3352607>.